PAPER

Visible light from modulated electron beam moving between twin circular silver nanowires forming plasmonic photonic molecule

IOP Publishing Journal of Optics
J. Opt. 22 (2020) 025002 (11pp) https://doi.org/10.1088/2040-8986/ab65d8

Visible light from modulated electron beam moving between twin circular silver nanowires forming plasmonic photonic molecule

Dariia O Yevtushenko and Sergii V Dukhopelnykov

Laboratory of Micro and Nano Optics, Institute of Radio-Physics and Electronics NASU, Kharkiv 61085, Ukraine

E-mail: dariia.yevtushenko@gmail.com

Received 5 August 2019, revised 11 November 2019
Accepted for publication 27 December 2019
Published 20 January 2020

Abstract

The visible-range diffraction radiation of harmonically modulated electron beam, which moves between twin circular silver nanowires, is considered. The electromagnetic field of such a two-dimensional beam is a surface wave propagating along its trajectory with the phase velocity equal to the beam velocity. This wave induces currents on the nanowires and hence radiation occurs even if the beam does not touch the wires. If the wires are tuned to a resonance, the radiated power displays a peak proportional to the resonant mode Q-factor. Sub-wavelength in radius silver nanowires are famous as nanoresonators due to the localized surface-plasmon modes. In our analysis, we use the field expansions in the azimuthal Fourier series and the addition theorems for the cylindrical functions. This enables us to reduce the wave scattering problem to a Fredholm second kind infinite-matrix equation that guarantees convergence of numerical solutions. Truncating this matrix, we compute the near and far field patterns of the wires as optically coupled plasmonic resonators and analyze dependence of the far-field spectral characteristics on the wavelength and electron beam parameters.

Keywords: optical diffraction radiation, silver nanowires, surface wave, plasmon resonance, total scattering cross-section, absorption cross-section

(Some figures may appear in colour only in the online journal)

1. Introduction

The effect of the visible-light radiation from the electron beams passing in vacuum over one-periodic relief gratings, across their grooves, is known since the 1950s when it was predicted and then verified experimentally [1]; later it was studied also in [2–4] and other publications, with applications mainly in the vacuum electronics. Today this effect is considered to be a particular case of more broadly defined phenomenon: the radiation that occurs if the charged particles or their beams excite nearby material objects without touching them, in various frequency regions. Such an effect is called diffraction radiation (DR) [5–14], in order to distinguish it from the transient radiation appearing when a particle crosses a boundary between different materials. Physically, the sources of DR are the surface and polarization currents induced on the scatterers placed in proximity to the beam trajectory.

Microwave-range DR is already in use as an attractive technique for non-invasive beam diagnostics, i.e. remote sensing of the beam position and velocity [10–14]. Such sensors are usually called beam position monitors (BPM). Today, BPM design can be extended to the optical range because emergence and rapid development of nanotechnology opens the way to fabricate ensembles of nanoscale optical scatterers with controlled shape and placement [15–17]. As nanosize components introduce negligible distortion to the beam, its velocity and trajectory can be assumed fixed. Then the analysis of DR effect can be done in the framework of

classical electromagnetic-wave scattering theory, i.e. as the scattering of the given wave by the scatterers of known shapes and material properties.

Performance of BPM greatly depends on its configuration, and it is quite natural that normally it uses a resonance to enhance the DR effect and, as a result, the BPM sensitivity. Nanosize scatterers are deeply sub-wavelength even in the visible range. There are two basic mechanisms to achieve electromagnetic-wave resonance at nanoscale. One implies the use of the lowest modes of high refractive index dielectric resonators and exploits the fact that the wavelength in material scales down as the inverse value of that index. Still, as the realistic values of refractive index are in the dozens and small hundreds, this mechanism offers the nanoscale cavities, which are rather sub-wavelength, i.e. still comparable to the free-space optical wavelength.

Recently, the work [18] presented a study of the pair of twin circular dielectric sub-wavelength wires made of appreciably high refractive index material as a sensor of the deviation of the modulated electron beam trajectory from the central position, between the wires. As was shown, non-zero shift of the beam is accompanied with appearance of additional sharp peaks in the total scattering cross-section (TSCS) spectra. The natural modes of such configurations are best understood as 'supermodes' built on the bonding and anti-bonding combinations of the modes of each wire. Then the additional peaks are associated with the bonding supermodes of such a photonic molecule, formerly 'dark' i.e. not excited by a symmetrically flowing beam of particles. The Q-factors of these modes can be high if the material of wires has small losses and, moreover, these Q-factors grow exponentially with refractive index and the wire radius.

The other mechanism to achieve a resonance at the nanoscale is associated with the use of the localized surface plasmon (LSP) modes of scatterers made of noble metals such as gold and silver. For the metal wires, LSP mode fields are H-polarized. If a sub-wavelength circular wire is placed into the free space, its LSP modes are clustered near to the wavelength λ where the following approximate quasi-static equation is held: $\mathrm{Re}\,\varepsilon(\lambda) = -1$, with $\varepsilon(\lambda)$ standing for the complex-valued dielectric function of metal [17, 19–22]. As one can see, this equation does not involve the wire radius, which can be formally arbitrarily small. The wavelengths, which satisfy this equation, are in the ultra-violet for silver and in the green for gold. However, even noble metals are sizably lossy in the visible range and hence the LSP Q-factors are quite low [17].

In the present work, we examine the configuration of twin circular silver wire as shown on figure 1. By the analogy with the photonic molecules made of dielectric particles, it can be viewed as a photonic plasmonic molecule with two-fold symmetry. Note that the plane-wave scattering from a twin-wire plasmonic scatterer was extensively studied in the past—see, for instance, [23–25]. Our goal is to analyze the visible-light DR from such a scatterer and to check how sensitive it is to a shift of the beam trajectory from the central-symmetric position and to a change of the beam velocity. This includes a detailed analysis of how the resonances on the coupled plasmonic modes of the twin silver wires are excited

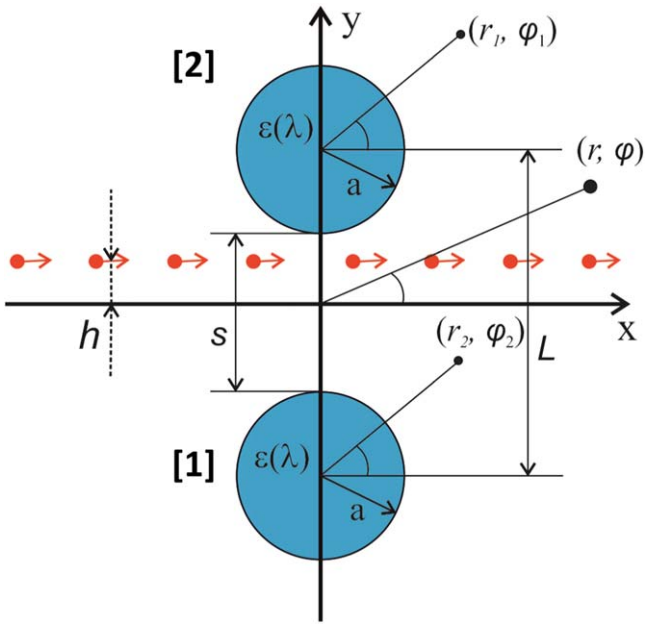

Figure 1. Cross-sectional geometry of a plasmonic photonic molecule made of two identical circular silver nanowires excited by a modulated electron beam moving between them.

by the modulated electron beam. Our work builds up on the preceding conference papers [26, 27], which have been considerably deepened and refined.

In section 2, we formulate the DR problem. Section 3 presents a brief review of the basic equations. Section 4 contains a summary of the equations for the scattering and absorption characteristics. In section 5, we explain how we characterize the dielectric function of silver. Numerical results are presented and discussed in section 6. The conclusions are summarized in section 7.

2. Problem formulation

Consider two identical circular silver nanowires (marked 1 and 2 in figure 1) separated by the distance L between their axes, with the same radius a and complex refractive index $\alpha(\lambda) = \sqrt{\varepsilon}$. We assume that the gap between the wires is $s = L - 2a$ and the Cartesian and the local, $(r_{1,2}, \varphi_{1,2})$, and the global, (r, φ), polar coordinates are chosen as shown in figure 1.

Consider now a one-dimensional (i.e. flat) electron beam moving along a straight trajectory at the distance $h > s/2$ from the x-axis, with a fixed velocity $v = \beta c$ ($\beta \leqslant 1$). The charge density function, if modulated in time in harmonic manner, can be presented as

$$\rho = \rho_0 \delta(y - h)\exp[i(kx/\beta - \omega t)], \qquad (1)$$

where $\delta(\cdot)$ is the Dirac delta function, ω and ρ_0 are the frequency and the amplitude of the beam modulation, $k = \omega/c$ is the free-space wavenumber, and c is the light velocity. In practical conditions, harmonic modulation of the electron beam can be arranged by its preliminary bunching in periodic waveguide or by using the direct laser illumination [11].

As shown in [2], the electromagnetic field of the beam (1) is an H-polarized slow wave compressed to the beam trajectory. Its magnetic field has a finite jump at the trajectory

$$H_z^0(x, y) = A\ \beta \mathrm{sign}(y - h) e^{-q|y-h|} e^{i(k/\beta)x}, \tag{2}$$

where $q = k\gamma/\beta$, $\gamma = (1 - \beta^2)^{1/2}$, function $\mathrm{sign}(\cdot) = \pm 1$ is the sign of the expression in the brackets, time dependence is omitted, and A is a known constant. Note that the field (2) decays exponentially in the normal to the trajectory direction, and the smaller β, the greater the field confinement at the trajectory. Besides, (2) has a finite jump at the beam trajectory that corresponds to the electric current.

In the presence of silver wires, the total magnetic field is different from (2). Neglecting the particles deceleration because of the loss of energy (this is called the given-current model), we can assume that the field (2) is fixed and consider it as the incident field. Then, to find the total field, we have to solve a 2D boundary-value wave-scattering problem. It involves the Helmholtz equation with coefficient k^2 or $k^2\alpha^2$ outside and inside the wires, respectively, the penetrable-boundary conditions at the wire contours (where the tangential field components, H_z and $E_{\varphi 1,2}$, must be continuous), the Sommerfeld radiation condition at infinity, and the condition of local power finiteness. These conditions guarantee the solution uniqueness.

3. Basic equations

Inside each wire, we expand the field in terms of the Fourier series in the local polar coordinate, φ_i, $i = 1, 2$,

$$H^{tot}(r, \varphi) = H^{(i)}(r_i, \varphi_i) = \sum_{m=-\infty}^{+\infty} y_m^{(i)} J_m(k\alpha r_i) e^{im\varphi_i}, \quad r_i < a, \tag{3}$$

where we have omitted the sub-index z. In the external domain, the total field can be presented as the sum of the incident field and the contributions from the twin scatterers

$$H^{tot} = H^0 + H^{ext}, \tag{4}$$

$$H^{ext}(r, \varphi) = \sum_{i=1,2} \sum_{m=-\infty}^{\infty} z_m^{(i)} H_m^{(1)}(kr_i) e^{im\varphi_i}, \quad r_i > a. \tag{5}$$

One of the boundary conditions requests he total field function H^{tot} to be continuous across each wire boundaries, $r_{1,2} = a$. On introducing the complex angles of incidence of the wave (2) above and below the beam trajectory, $\psi_{1,2}$, such that

$$\cos\psi_{1,2} = 1/\beta, \quad \sin\psi_{1,2} = \pm i\gamma/\beta, \tag{6}$$

and using the Jacobi–Anger formula in the complex domain, we can expand the incident field in terms of the azimuth series in the local coordinates of each wire as in [5]

$$\begin{aligned} H^0(r_{1,2}, \varphi_{1,2}) &= \mp A\beta e^{-q(L/2\pm h)} e^{ikr_{1,2}\cos\psi_{1,2}} \\ &= \mp A\beta e^{-q(L/2\pm h)} \sum_{m=-\infty}^{+\infty} i^m J_m(kr_{1,2}) \\ &\times \left(\frac{1 \mp \gamma}{\beta}\right)^m e^{im\varphi_{1,2}}. \end{aligned} \tag{7}$$

Then, substituting (4), (5), and (7) into the boundary condition for H^{tot} and using the orthogonality of exponents, we obtain the following connection between the unknown expansion coefficients:

$$\begin{aligned} y_m^{(1,2)} J_n(k\alpha a) &= z_m^{(1,2)} H_m(ka) \\ &+ \sum_{n=-\infty}^{+\infty} (\mp i)^{(n-m)} z_n^{(2,1)} J_n(ka) H_{m-n}(kL) + f_m^{(1,2)}, \end{aligned} \tag{8}$$

where $J_m(\cdot)$ and $H_m(\cdot)$ are the Bessel and the first-kind Hankel functions, respectively, the upper index, (1), of the latter is omitted for brevity, and

$$f_m^{(1,2)} = \mp A\beta e^{-q(L/2\pm h)} i^m J_m(ka)(1 \mp \gamma)^m \beta^{-m}. \tag{9}$$

Expression (8) can be used to eliminate the coefficients $y_m^{(1,2)}$ from the other boundary condition, which requires the continuity of the function $E_{\varphi 1,2}^{tot} = (Z_0/ik\varepsilon)\partial H^{tot}/\partial r_{1,2}$ across each wire boundary (where $Z_0 = (\mu_0/\varepsilon_0)^{1/2}$ is the free-space impedance). Then, on introducing new unknowns $\tilde{z}_m^{(1,2)} = z_m^{(1,2)} w_m$, where $w_m = m!(2/ka)^m$, and doing some algebra, we arrive at the following coupled infinite-matrix equations for the latter coefficients:

$$\tilde{z}_m^{(i)} + \sum_{n=-\infty}^{+\infty} A_{mn}^{(ij)} \tilde{z}_n^{(j)} = B_m^{(i)}, \quad m = 0, \pm 1, \pm 2, \ldots, \tag{10}$$

$$A_{mn}^{(ij)} = (\mp i)^{(n-m)} J_n(ka) V_m^{(i)} H_{m-n}(kL)(P_m^{(i)})^{-1}, \tag{11}$$

$$B_m^{(i)} = -[f_m^{(i)}(ka) J'_m(k\alpha a)\alpha_i - k^{-1} J_m(k\alpha a) f'^{(i)}_m(ka)](P_m^{(i)})^{-1}, \tag{12}$$

$$V_m = \alpha J_m(ka) J'_m(k\alpha a) - J'_m(ka) J_m(k\alpha a), \tag{13}$$

$$P_m = w_m[\alpha H_m(ka) J'_m(k\alpha a) - H'_m(ka) J_m(k\alpha a)], \tag{14}$$

where $i, j = 1, 2$, $i \neq j$, and the prime stands for the differentiation in argument.

This is the same equation set as derived earlier in [18] in the analysis of DR in the presence of twin circular wires made of high refractive index dielectric material. Note that, thanks to the introduction of the scaled coefficients $\tilde{z}_m^{(1,2)}$, the matrix operator in (10) is compact (similar scaling was also used in [28–31] for the scattering by other finite and infinite collections of circular wires). This scaling is crucially important as it is only in such case that the Fredholm theorems guarantee that numerical solution of (10), truncated to finite order M, converges to the exact solution as $M \to \infty$.

The following empirical rule has been found: to obtain five effective digits in the near field, one has to take $M \geqslant k\alpha a + 5$ (and more if the gap $s < 0.01a$). We use this rule when computing the results presented in the next section.

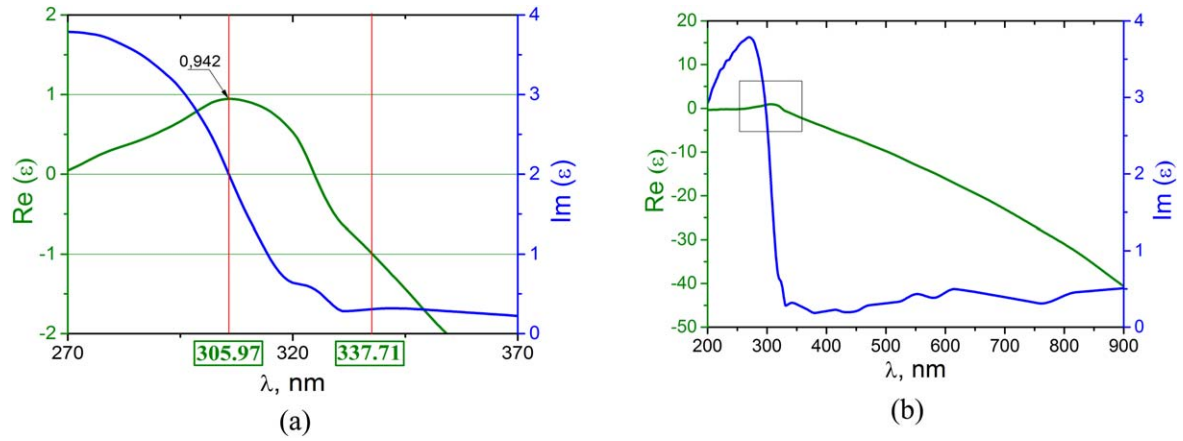

Figure 2. Bulk complex relative permittivity function of silver versus the wavelength in the optical range (a), and its zoom in a gray-boundary ultra-violet domain (b).

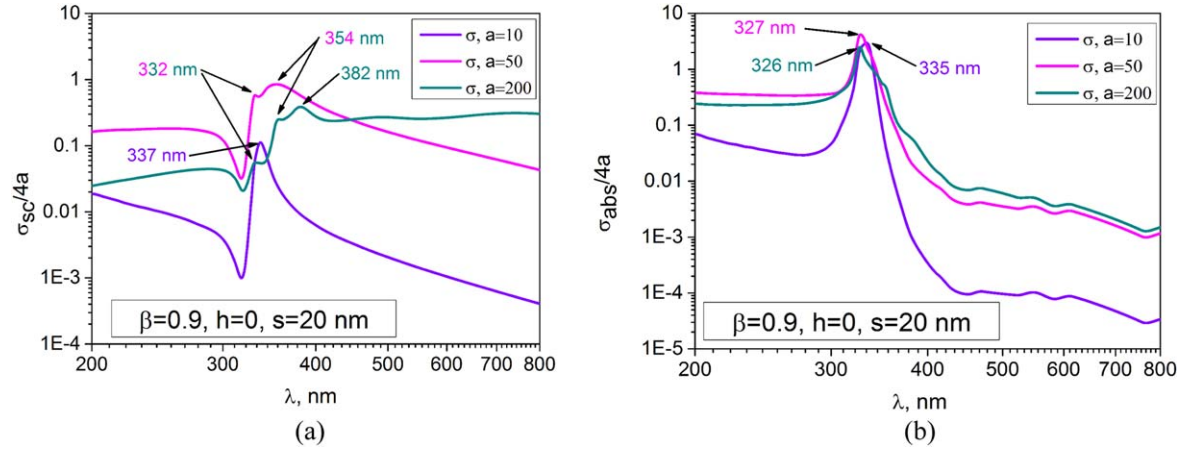

Figure 3. Normalized TSCS (a) and TACS (b) of two identical silver nanowires versus the wavelength, for the electron beam with the relative velocity $\beta = 0.9$ flowing along the x-axis ($h = 0$).

4. Scattering and absorption characteristics

Far from the wires, at $r \to \infty$, the scattered field behaves asymptotically as a cylindrical wave, $H^{ext}(r, \varphi) = (2/i\pi kr)^{1/2}\Phi(\varphi)\exp(ikr)$, that can be derived from (5) with the aid of the large-argument asymptotic expressions for the Hankel functions. Here, the far-field angular pattern is a function of the coefficients $z_m^{(1,2)}$,

$$\Phi(\varphi) = \Phi_1(\varphi) + \Phi_2(\varphi), \quad \Phi_{1,2}(\varphi) = \exp\left(\mp\tfrac{1}{2}ikL\sin\varphi\right) \times \sum_{m=-\infty}^{+\infty}(-i)^m J_m(ka)\tilde{z}_m^{(1,2)}\exp(im\varphi), \tag{15}$$

Note that the series in (15) converge exponentially as soon as $|m|$ becomes larger than ka. In the case of DR analysis, the scatterers can be located in either of two half-spaces. We assume that the beam travels away from the wires, that is, $h < s/2$. Then, it is convenient to present the TSCS as a sum of two partial SCS, into the lower and the upper half-spaces, respectively

$$\sigma_{sc} = \sigma_{sc}^{(1)} + \sigma_{sc}^{(2)}. \tag{16}$$

They are found from the integration of the normal component of the time-averaged Poynting vector over the corresponding semi-circles of large radius

$$\sigma_{sc}^{(1,2)} = \frac{2}{\pi kA^2}\int_0^{\mp\pi}|\Phi(\varphi)|^2\, d\varphi. \tag{17}$$

As the silver is lossy, the incident field is not only scattered but also absorbed in the wires. The figure of merit of this effect is the total absorption cross-section (TACS). The TACS can be found from the integration of the electric-field power over the wire cross-section areas or, equivalently, from the integration of the normal component of the time-averaged Poynting vector over the contours of the wires. For metals, the former way involves differentiation of the dielectric function, $\varepsilon(\lambda) = \alpha^2(\lambda)$, in wavelength. As we do not want to use the Drude approximation for the dielectric function of silver and, instead, use experimental data of [32], this differentiation can be done only numerically. Therefore, the latter way is more suitable as it avoids such an operation. The corresponding expressions take the following form:

$$\sigma_{abs} = \sigma_{abs}^{(1)} + \sigma_{abs}^{(2)}, \tag{18}$$

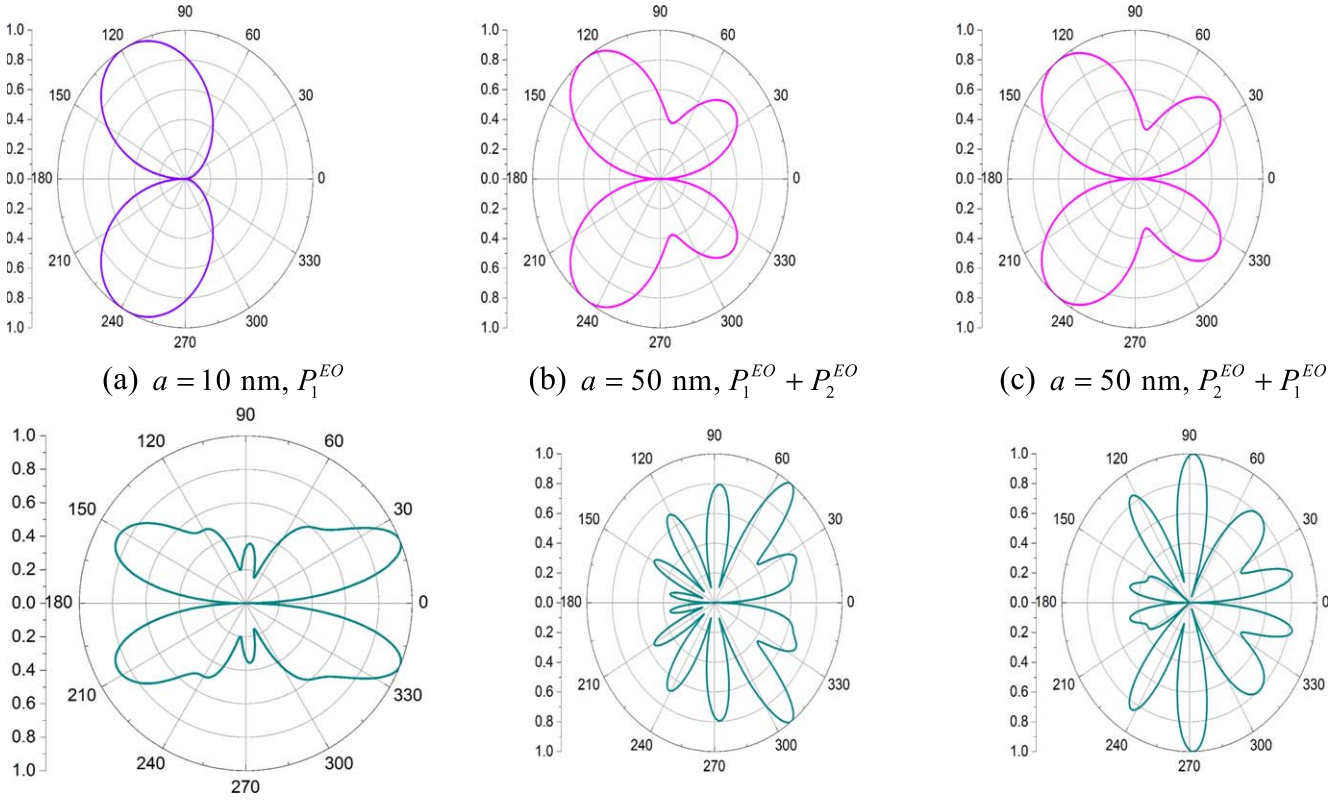

Figure 4. Normalized far-field scattering patterns of the twin silver nanowires for the beam flowing along the x-axis ($h = 0$) with the relative velocity $\beta = 0.9$. The wire radius is as indicated, and the wavelength is $\lambda = 337$ nm (a), 332 nm (b), 354 nm (c), 332 nm (d), 354 nm (e), and 382 nm (f).

$$\sigma_{abs}^{(1,2)} = \frac{2\pi a}{|\alpha|^2 A^2} \sum_{m=-\infty}^{\infty} |y_m^{(1,2)}|^2 \mathrm{Im}[\alpha J_m(k\alpha a) J_m'(k\alpha^* a)], \quad (19)$$

where * means the complex conjugate.

The sum $\sigma_{sc} + \sigma_{abs}$ is the extinction cross-section, σ_{ext}. In the plane wave scattering, this quantity is linked to the far-field scattering pattern magnitude in the forward direction by the expression known as optical theorem. In our case, we have the surface wave (2) as the incident field. Still, a similar expression can be derived using the complex angles of incidence $\psi_{1,2}$ above and below the beam trajectory, as defined in (6), and substituting them into the complex Poynting theorem. Extracting the real part, we find that

$$\sigma_{ext} = \sigma_{sc} + \sigma_{abs} = -\frac{4}{kA^2} \mathrm{Re}\,[\Phi_1(\psi_1) + \Phi_2(\psi_2)] \quad (20)$$

or, with account of (15)

$$\sigma_{sc} + \sigma_{abs} = -\frac{4}{kA^2} e^{-qL/2}\,\mathrm{Re} \sum_{m=-\infty}^{+\infty} (-i^m) J_n(ka) \left[z_n^{(1)} e^{-qh} \left(\frac{1-\gamma}{\beta} \right)^m + z_n^{(2)} e^{qh} \left(\frac{1+\gamma}{\beta} \right)^m \right]. \quad (21)$$

The obtained expression is the optical theorem for DR excited by the beam (1) flowing between the wires of plasmonic PM. Fulfillment of (21) provides partial validation of the solution correctness, although full validation needs the verification of the fulfillment of the boundary conditions.

As we have verified, the error in the optical theorem oscillates at the level of machine precision and the error in the boundary conditions is the same level as for the solution of (10), controlled by the matrix truncation order M. Additionally, if we set the material of wire #2 to be the free space, then the computed cross-sections coincide with their values for a stand-alone silver wire, found in analytical form [17].

In the computations, we assume, without a loss of generality, that the constant $A = 1\ \mathrm{A\,m^{-1}}$.

5. Dielectric function of silver

The Johnson and Christy experimental data [26] are adopted to incorporate the wavelength-dependence optical response of bulk silver, $\varepsilon(\lambda)$, interpolated in the same way as in [17]. The spectra of the real and imaginary parts of that function in the ultra-violet range are shown in figure 2(a), and in figure 2(b), the same is shown in the whole visible-light range. Note that the Drude formula, being a reasonable approximation at longer waves, fails to provide accurate characterization in the ultra-violet.

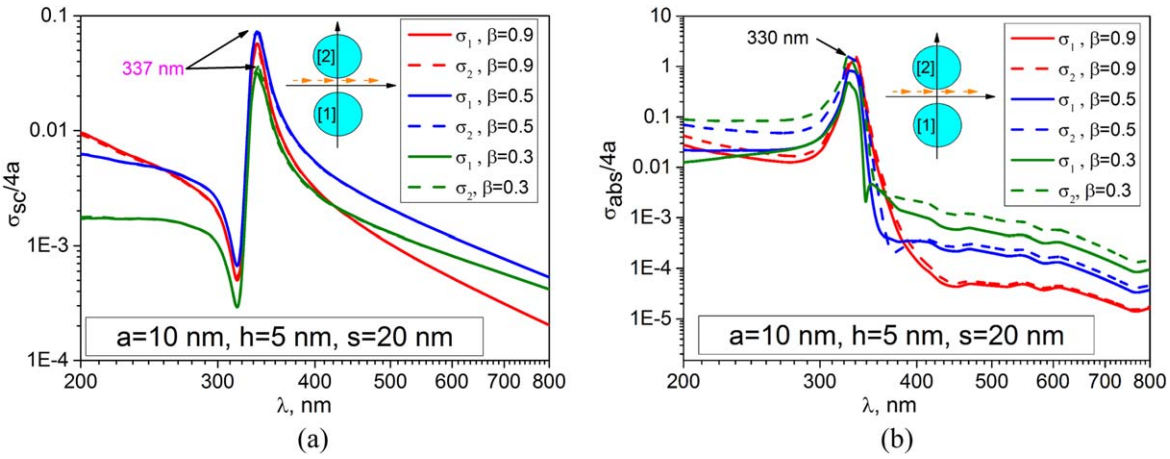

Figure 5. Normalized partial SCS of twin silver nanowires with radius 10 nm versus the wavelength in the visible range, for several values of the electron velocity β. The beam flows above the x-axis at the distance $h = 5$ nm.

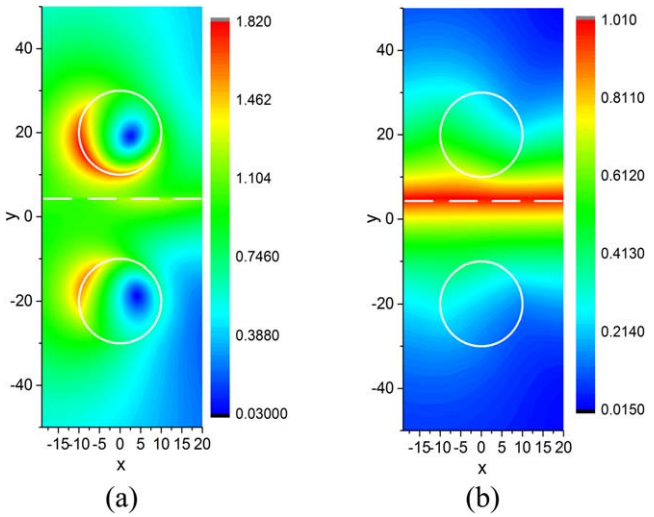

Figure 6. Normalized near magnetic field patterns of the 10 nm in radius twin silver nanowires excited with the electron beam having the velocity $\beta = 0.3$, in the plasmon resonance at $\lambda = 337$ nm (a) and in the 'quasi-invisibility' case (minimum scattering) at $\lambda = 330$ nm (b). The beam flows above the x-axis: $h = 5$ nm.

As one can see, there are two remarkable wavelengths, both laying in the ultra-violet. One is around 306 nm where $\mathrm{Re}\,\varepsilon = 0.942$ that is quite close to $+1$. This means that silver is optically well-transparent at this wavelength although the losses remain significant as $\mathrm{Im}\ \varepsilon = 1.97$. Note that this effect of 'quasi-invisibility' cannot be reproduced with the Drude formula for the dielectric function of silver. This justifies our choice of the Johnson and Christy data in the analysis of silver scatterers of the visible light.

The other important wavelength value is around 337.7 nm, where $\mathrm{Re}\,\varepsilon = -1$. This is the approximate quasi-static 'text-book' value for the collective resonance on the LSP modes of a single circular metal wire in the free space [14, 16–19]. It is valid if the losses can be neglected, $\mathrm{Im}\ \varepsilon = 0$. Although for silver $\mathrm{Im}\ \varepsilon = 0.3$ at that wavelength, it predicts the peak of absorbance and scattering within the 5% accuracy if the silver wire is thinner than 10 nm in radius.

6. Numerical results

Figure 3 demonstrates the dependences of the normalized by $4a$ TSCS and TACS (sum of (17) and (19), respectively) on the electron-beam modulation wavelength in the visible range, for twin silver nanowires with sub-wavelength radius values $a = 10$, 50, and 200 nm, separated by the gap of $s = 20$ nm between them. The beam flows along the x-axis (i.e. symmetrically, so that the shift is $h = 0$) and the beam velocity is $\beta = 0.9$ that corresponds to so-called relativistic beam.

The plots of TSCS show one, if $a = 10$ nm, or a few, if a is lager, peaks. This peak is known as collective resonance on the LSP modes of thin silver twin nanowires. In [14], it was already demonstrated that the plasmon resonance on a stand-alone metal wire can be excited not only by an H-polarized plane wave as in [28–32] but also by a modulated electron beam.

The photonic-plasmonic molecule built of twin circular metal nanowires is a more complicated open plasmonic resonator. Its natural modes have much in common with the modes of the photonic molecule built of two circular dielectric disks or wires, studied in [18, 28]. They form so-called 'plasmonic supermodes' built on optically coupled LSP modes of each wire. In the case of twin wires these supermodes make quartets where each of them belongs to one of four independent classes of symmetry of the pair [18, 28]. They can be, therefore, denoted as P_m^{EE}, P_m^{OE}, P_m^{EO}, P_m^{OO}, where $E(O)$ corresponds to the even (odd) dependence on x and y.

Note that similarly to the plane-wave scattering from a single circular silver wire [22], for the thicker wires the LSP peak in the scattering cross-section splits to several ones, where the most red-shifted peak corresponds to the

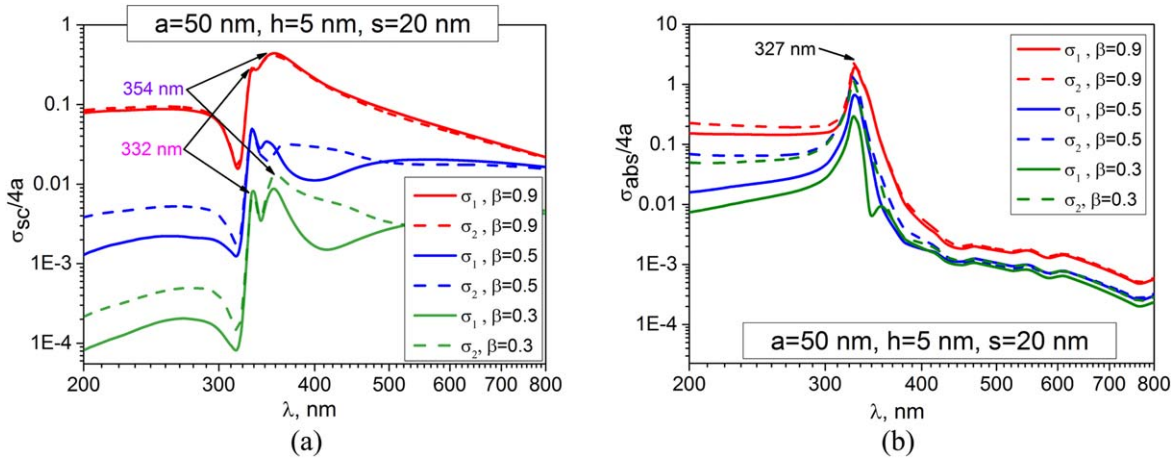

Figure 7. The same as in figure 2 however for the wire radius 50 nm.

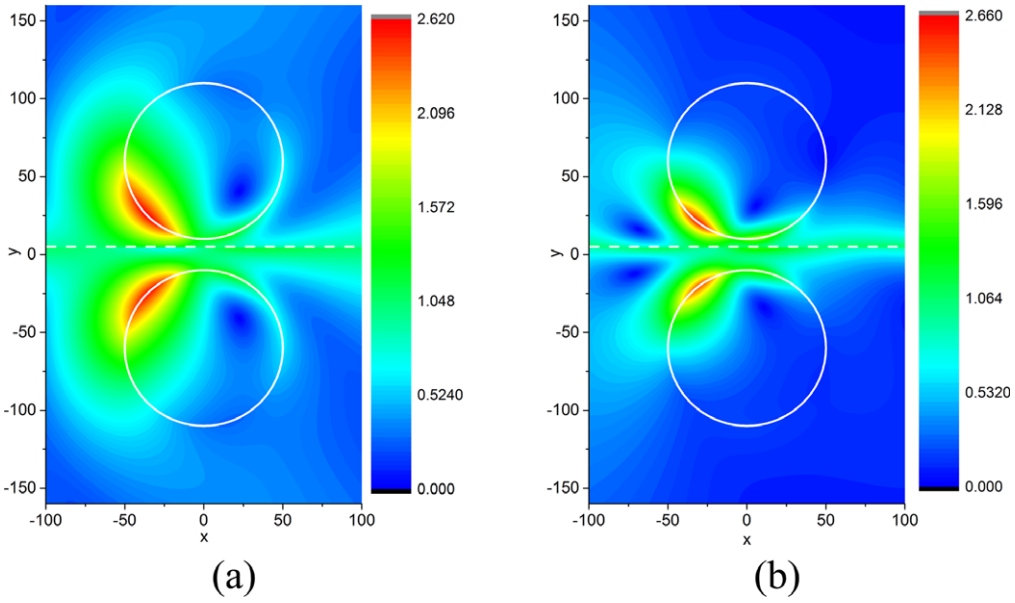

Figure 8. Normalized near magnetic field patterns of the 50 nm in radius twin silver nanowires at $\lambda = 332$ nm for the electron beam velocity $\beta = 0.9$ (a) and $\beta = 0.3$ (b); the beam flows above the x-axis ($h = 5$ nm).

supermode built on the P_1 mode of each wire, and others correspond to the supermodes on the higher-order LSP modes. In view of the symmetry, partial SCS are each equal to one-half of TSCS.

In contrast, the plots of TACS of a deeply sub-wavelength silver wire demonstrate only one common peak, slightly blue-shifted for the thicker wires from the quasi-static value of 337 nm. The higher-order LSP resonances show up as gentle 'shoulders' on the red side of that peak.

The effect of 'quasi-invisibility' is present on the plots of TSCS for both thin and thick silver wires (note that this phenomenon has no relation to 'Fano-shape' resonances in the other scattering analyses). The associated minimum is especially deep for a deeply sub-wavelength wire. On the plots of TACS, there is no similar minimum due to considerable losses in the bulk silver.

In figure 4, we present the normalized far-field scattering patterns at the wavelengths of the peaks on the TSCS plots of figure 3(a). As the beam flows strictly in the middle between the wires, the angular patterns have zeros along the x-axis. The number of lobes in the far zone corresponds to the mode index m.

Now, to clarify the effect of the shift of the beam trajectory on the scattering and absorption, we show the visible-range spectra of the partial TCS and ACS for several values of the silver wire radius a and the gap of 20 nm however assuming that $h = 5$ nm. To see what changes if the beam velocity β varies, we select it as 0.3, 0.5 and 0.9.

The plots in figure 5(a) demonstrate the dependences of the normalized by $4a$ partial SCS on the modulation wavelength in the visible range, for nanowires with deeply sub-wavelength radius of $a = 10$ nm. As one can see, for all

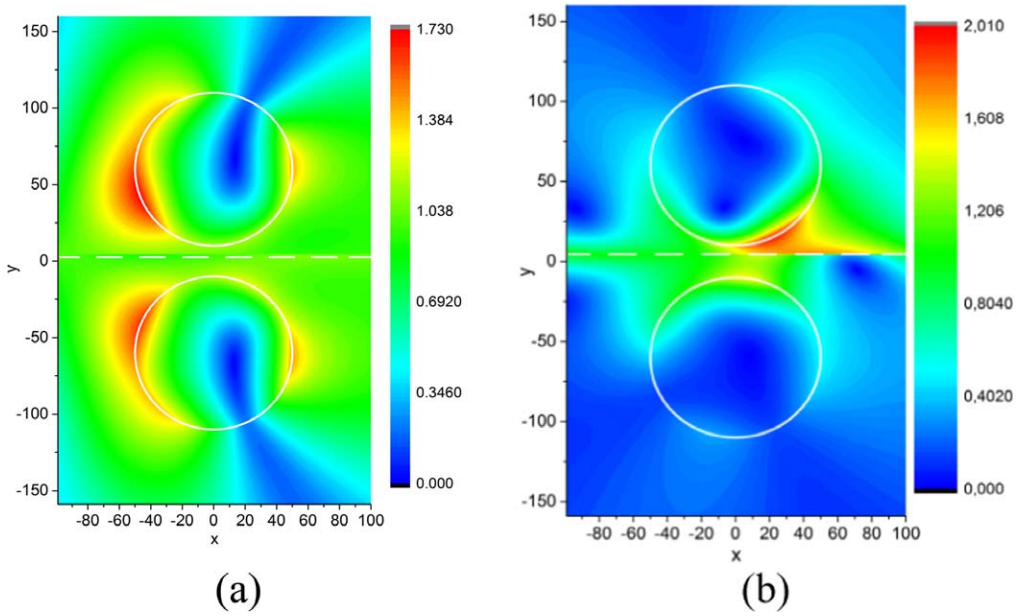

Figure 9. The same as in figure 5 however at $\lambda = 354$ nm (i.e. at the shoulder on the TSCS plots) for the beam velocity $\beta = 0.9$ (a) and $\beta = 0.3$ (b); the beam shift is $h = 5$ nm.

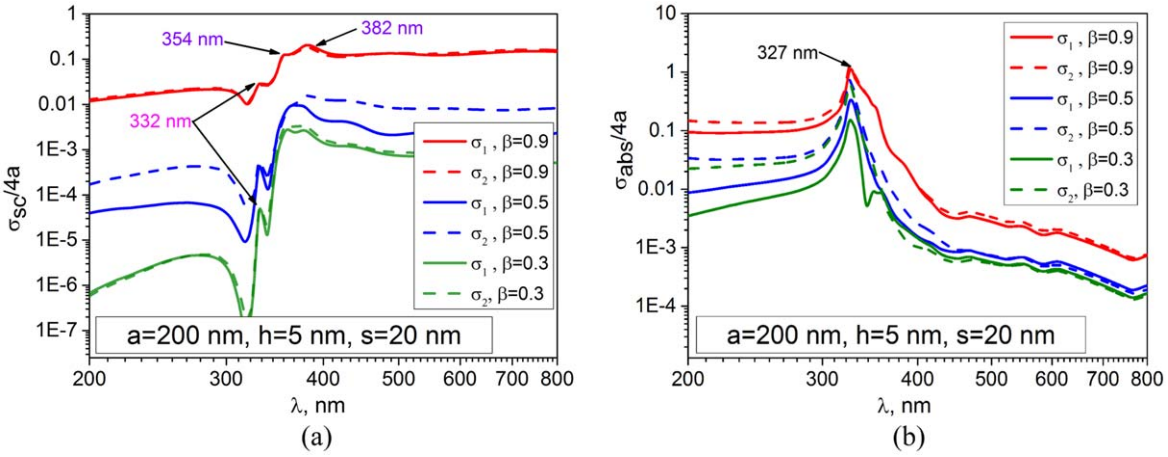

Figure 10. The same as in figures 2 and 4, however for the wire radius 200 nm.

values of β, the plots of partial SCS, $\sigma_{sc}^{(1)}(\lambda)$ and $\sigma_{sc}^{(2)}(\lambda)$, are very close to each other. They show one distinctive peak at $\lambda = 337$ nm that does not change its place noticeably if the beam shift h gets larger. The effect of the 'quasi-invisibility' is also well visible as a deep minimum, slightly red-shifted from the value of 306 nm where the bulk silver dielectric function is closest to $+1$.

In the absorption (figure 5(b)), the LSP peak appears at a slightly blue-shifted position between 330 and 335 nm, depending on the velocity β and shift value h. As already mentioned, there is no 'invisibility' effect in the absorption as the silver is heavily lossy in the deep ultra-violet. Note that the partial TCSs of such thin nanowires are practically the same for any beam velocity β. The plots of ACS demonstrate a similar independence of β for relativistic beams, however, if β becomes smaller, the difference in favor of the nearer wire becomes visible.

Color maps in figure 6(a) demonstrate in-resonance patterns of the near magnetic field for such deeply sub-wavelength wires. Figure 6(a) corresponds to the peak in the scattering. One can conclude that the near field is dominated by the contribution of two nearly degenerate supermodes, P_1^{EO} and P_1^{OO}. The field in figure 6(b) corresponds to the 'scattering invisibility' wavelength. It shows, indeed, that in this case the beam of particles does not see the silver nanowires as its field is very close to the field (2) in the free space.

For the better insight into the physics of DR, the plots in figure 7 present the spectra of the partial SCS and ACS for the beam-excited twin silver nanowires of larger radius, 50 nm.

Unlike the thinner wires, these configurations show, besides of the main peak, several smaller ones at the longer wavelengths. They are well resolved on the SCS plots and correspond to the *EO* supermodes built on the higher-order LSP modes P_m of each circular wire (see [17, 21]). This is

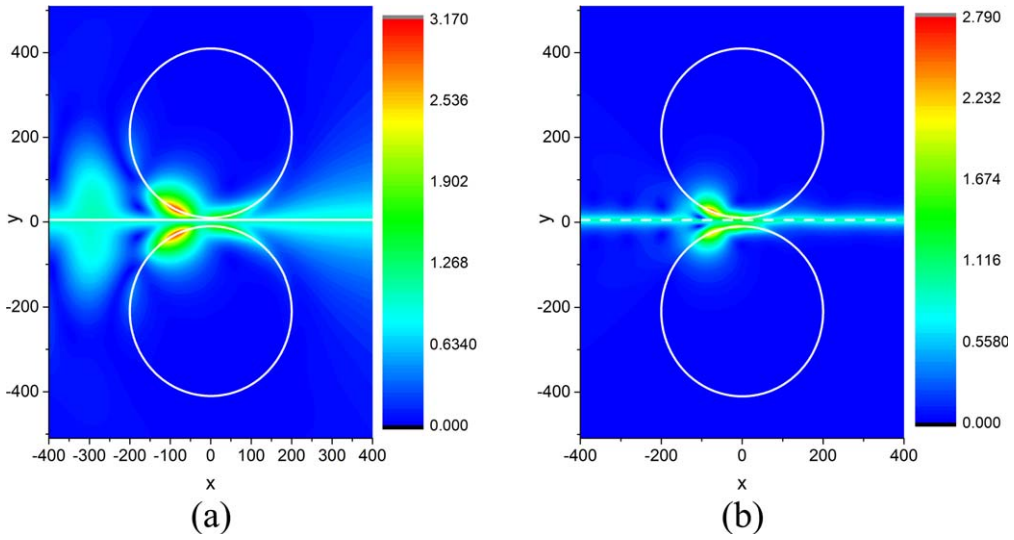

Figure 11. Near magnetic field patterns of the 200 nm in radius twin silver nanowires at $\lambda = 332$ nm (the most 'violet' peak), for the electron beam velocity $\beta = 0.9$ (a) and $\beta = 0.3$ (b); the beam flows above the x-axis ($h = 5$ nm).

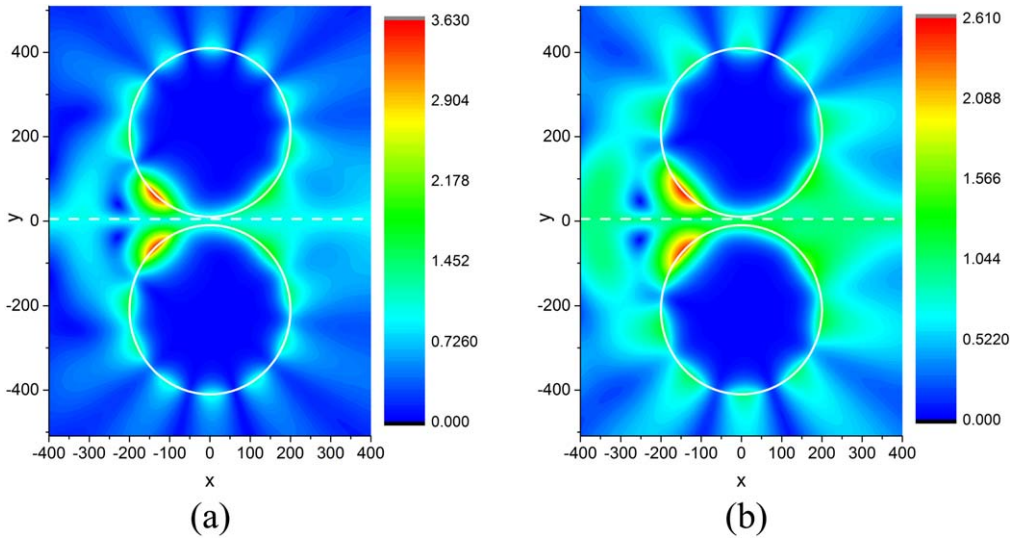

Figure 12. The same as in figure 8 however in the smaller peaks of TSCS in figure 7, that is at $\lambda = 354$ nm (a) and $\lambda = 382$ nm (b). The electron beam is relativistic, $\beta = 0.9$, and flows above the x-axis, $h = 5$ nm.

clearly visible in the near-field patterns corresponding to these additional peaks, shown in figures 8 and 9. Note that the field asymmetry is clearly visible only in figure 8(b) and especially in figure 9(b), where $\beta = 0.3$, and if $\beta = 0.9$, then it is alleviated by the slower decay of the incident field away from the trajectory. The plots in figure 10 correspond to even larger wires of $a = 200$ nm. The patterns in figures 11 and 12 show that the near field is dominated by the LSP supermode mode P_m^{EO} with $m = 5$ (a) and $m = 4$ (b). The interpretation is also supported by the far-field angular scattering patterns, presented in figure 4. The plots of partial cross-sections show that, unlike thinner wires, the thicker ones demonstrate that nearer to the beam wire is both a stronger scatterer and a stronger absorber unless the beam is relativistic (that is if $\beta \to 1$), although for the 200 nm wire the near field patterns are almost symmetric.

In order to obtain clearer vision of the effect of asymmetry in the light scattering and absorption, which appears in the studied configuration if the beam trajectory is shifted from the central position, we have computed the spectra of the scattering and extinction asymmetry factor. The latter quantities are introduced in the following manner:

$$\xi_{sc} = \frac{\sigma_{sc}^{(2)} - \sigma_{sc}^{(1)}}{\sigma_{sc}^{(2)} + \sigma_{sc}^{(1)}}, \qquad \xi_{ext} = \frac{\sigma_{ext}^{(2)} - \sigma_{ext}^{(1)}}{\sigma_{ext}^{(2)} + \sigma_{ext}^{(1)}}. \tag{22}$$

The results of our calculations are presented in figure 13.

As one can see, a shift of the beam trajectory towards the upper wire results in a generally stronger scattering into the upper halfspace and a larger extinction in this halfspace. This is expected behavior in view of the exponential decay of the beam field (2) in the normal to the trajectory direction. Still the dependence of the asymmetry factors on the shift distance

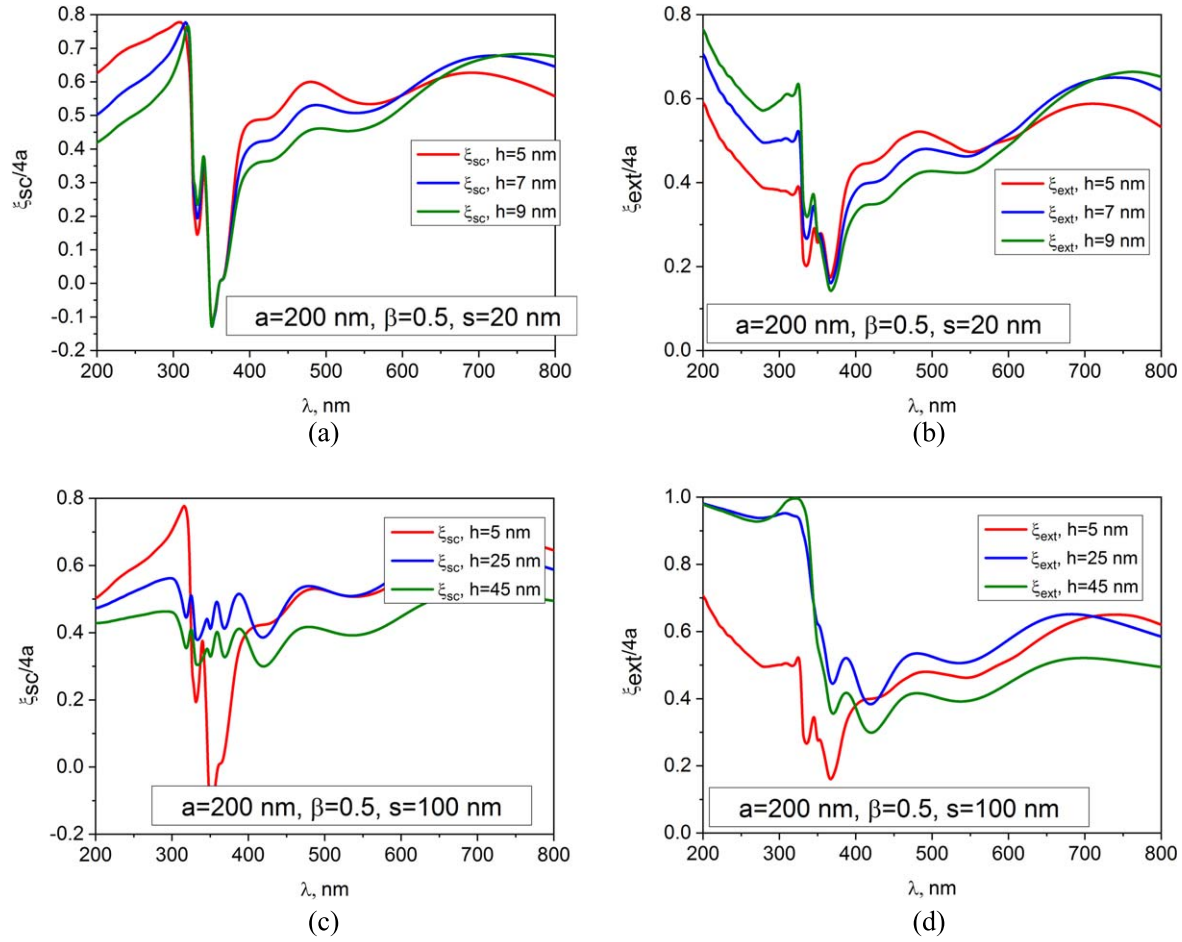

Figure 13. The scattering (a), (c) and extinction (b), (d) asymmetry factors for the wires of the radius 200 nm, the electron beam velocity $\beta = 0.5$, and the airgap of $s = 20$ nm (a), (b) and $s = 100$ nm (c), (d).

is a complicated function of various parameters including the frequency.

7. Conclusions

The electromagnetic field of a modulated electron beam is a slow wave propagating along the beam trajectory, with exponential decay away from it. This wave induces surface and polarization currents on the neighboring obstacles that radiate into the outer space even if the beam does not touch them. We have studied, for the first time to the best of our knowledge, how the visible-light DR is emitted by a beam, moving between a pair of identical circular silver nanowires. As we have found, they behave as optically coupled plasmonic open resonators. Because of the losses in silver, their LSP supermodes (that is, hybrid modes) have rather low Q-factors however are still able to enhance the DR at the corresponding wavelengths. If the beam trajectory shifts away from the central (symmetrical) position between the silver wires, then the near field pattern also loses symmetry. This is better visible if the wire radius is truly sub-wavelength and the beam is non-relativistic. Still, unlike a pair of high refractive index dielectric nanowires [18], the low values of LSP mode Q-factors and their clustering near to the same wavelength show that the solid circular metal wires are not the optimum shape for the applications related to the optical beam-position monitors. Therefore, additional studies are needed to explore the opportunities of configurations, which support LSP resonances with higher Q-factors, for instance, made of a pair of hollow thin-wall metal nanotubes.

ORCID iDs

Dariia O Yevtushenko https://orcid.org/0000-0001-6569-1226
Sergii V Dukhopelnykov https://orcid.org/0000-0002-0639-988X

References

[1] Smith S J and Purcell E M 1953 Visible light from localized surface charges moving across a grating *Phys. Rev.* **92** 1069
[2] Sologub V G *et al* 1968 Excitation of an electromagnetic field by an electron beam traveling close to a diffraction grating *Radiophys. Quantum Electron.* **11** 327–33

[3] van den Berg P M 1973 Smith-Purcell radiation from a line charge moving parallel to a reflection grating *J. Opt. Soc. Am.* **63** 689–98
[4] Potylitsyn A P 1998 Resonant diffraction radiation and Smith–Purcell effect *Phys. Lett.* A **238** 112–6
[5] Nosich A I 1981 Diffraction radiation which accompanies the motion of charged particles near an open resonator *Radiophys. Quantum Electron.* **24** 696–701
[6] Pazynin L A and Sologub V G 1982 Radiation of a point charge moving uniformly along the axis of a narrow cylindrical ring *Radiophys. Quantum Electron.* **25** 64–8
[7] Pazynin L A and Sologub V G 1984 Diffraction radiation of a point charge moving along the axis of a segment of a circular waveguide *Radiophys. Quantum Electron.* **27** 816–22
[8] Pazynin L A and Sologub V G 1987 Excitation of a cylindrical retarding system of finite length by a modulated flux of charge particles *Radiophys. Quantum Electron.* **30** 376–87
[9] Boltonosov A I and Sologub V G 1988 Excitation of an open strip-type resonator by a modulated beam of charged particles *Sov. J. Communic. Technol. Electron.* **33** 133–40
[10] Castellano M 1997 A new non-intercepting beam size diagnostics using diffraction radiation from a slit *Nucl. Instrum. Methods Phys. Res.* A **394** 275–80
[11] Castellano M 2001 Measurements of coherent diffraction radiation and its application for bunch length diagnostics in particle accelerators *Phys. Rev.* E **63** 056501
[12] Karataev P *et al* 2004 Beam-size measurement with optical diffraction radiation at KEK accelerator test facility *Phys. Rev. Lett.* **93** 244802
[13] Goponov Y A, Shatokhin R A and Sumitani K 2018 Diffracted diffraction radiation and its application to beam diagnostics *Nucl. Instrum. Meth. Phys. Res.* A **885** 134–8
[14] Bobb L *et al* 2018 Feasibility of diffraction radiation for noninvasive beam diagnostics as characterized in a storage ring *Phys. Rev. Accel. Beams* **21** 03801
[15] Muto T *et al* 2003 Observation of incoherent diffraction radiation from a single-edge target in the visible-light region *Phys. Rev. Lett.* **90** 104801–4
[16] Talebi N 2017 Interaction of electron beams with optical nanostructures and metamaterials: from coherent photon sources towards shaping the wave function *J. Opt.* **19** 103001
[17] Yevtushenko D O, Dukhopelnykov S V and Nosich A I 2019 Modeling of optical diffraction radiation from a dielectric and a silver nanowire excited by a modulated electron beam *Opt. Quantum Electron.* **51** 29
[18] Yevtushenko D O, Dukhopelnykov S V and Nosich A I 2019 Electron-beam excitation of supermodes of a photonic molecule built on twin high refractive index dielectric nanowires *J. Appl. Phys.* **125** 223102
[19] Bohren C F and Huffman D R 2004 *Absorption and Scattering of Light by Small Particles* (Weinheim: Wiley)
[20] Novotny L and Hecht B 2012 *Principles of Nano-Optics* (Cambridge: Cambridge University Press)
[21] Lukyanchuk B S and Ternovsky V 2006 Light scattering by a thin wire with a surface-plasmon resonance: bifurcations of the poynting vector field *Phys. Rev.* B **73** 235432
[22] Velichko E A and Natarov D M 2018 Localized versus delocalized surface plasmons: dual nature of resonances on a silver circular wire and a silver tube of large diameter *J. Opt.* **20** 075002/9
[23] Kottmann J P and Martin O J F 2001 Retardation-induced plasmon resonances in coupled nanoparticles *Opt. Lett.* **26** 1096–8
[24] Kottmann J P and Martin O J F 2001 Plasmon resonant coupling in metallic nanowires *Opt. Express* **8** 655–63
[25] Natarov D M, Sauleau R and Nosich A I 2012 Periodicity-enhanced plasmon resonances in the scattering of light by sparse finite gratings of circular silver nanowires *IEEE Photonics Technol. Lett.* **24** 43–5
[26] Yevtushenko D O and Dukhopelnykov S V 2019 Near fields of twin circular silver nanowires exited by electron beam moving between them *Proc. Int. Conf. Electronics and Nanotechnology (ELNANO-2019), Kyiv* pp 340–3
[27] Yevtushenko D O and Dukhopelnykov S V 2019 Total scattering cross-section of twin circular silver nanowires exited by electron beam moving between them *Proc. European Microwave Conf. Central Europe (EuMCE-2019), Prague* pp 386–9
[28] Smotrova E I *et al* 2006 Optical coupling of whispering-gallery modes in two identical microdisks and its effect on photonic molecule lasing *IEEE J. Sel. Top. Quant. Electron.* **12** 78–85
[29] Natarov D M *et al* 2011 Periodicity-induced effects in the scattering and absorption of light by infinite and finite gratings of circular silver nanowires *Opt. Express* **19** 22176–90
[30] Natarov D M *et al* 2014 Effect of periodicity in the resonant scattering of light by finite sparse configurations of many silver nanowires *Plasmonics* **9** 389–407
[31] Zinenko T L *et al* 2016 Grating resonances on periodic arrays of sub-wavelength wires and strips: from discoveries to photonic device applications *Contemporary Optoelectronics: Materials, Metamaterials and Device Applications* ed O Shulika and I Sukhoivanov vol 199 (Berlin: Springer) pp 65–79
[32] Johnson P B and Christy R W 1972 Optical constants of the noble metals *Phys. Rev.* B **6** 4370–9